Normal and superconducting state properties of Cu-doped FeSe single crystals

Chunsheng Gong (龚春生), Shanshan Sun (孙珊珊), Shaohua Wang (王少华), and Hechang Lei (雷和畅)*
Department of Physics and Beijing Key Laboratory of Opto-electronic Functional Materials and Micro-nano Devices, Renmin University of China, Beijing 100872, China

(Received 1 December 2020; revised 27 April 2021; accepted 4 May 2021; published 18 May 2021)

We report the evolution of the physical properties of FeSe single crystals with Cu substitution. We show that introducing Cu suppresses bulk superconductivity quickly, much faster than the decrease in structural transition temperature, and further doping Cu induces a metal-insulator transition. In contrast, zero-field *ab*-plane resistivity ρ_{xx} exhibits an unusual temperature dependence $\rho_{xx}(T) \sim AT^n$, with $n \sim 1$, that is almost unchanged with the variation of Cu content. This result implies that magnetic fluctuations in FeSe are insensitive to the Cu substitution. The field dependence of the Hall resistivity of $Fe_{1-x}Cu_xSe$ with $x > 0$ shows a positive slope in the low-temperature region which can be ascribed to the relatively higher hole mobility than the electron one. Therefore, the low-concentration Cu dopant as a strong scattering source can lead to the significant decrease in electron mobility which is detrimental to superconductivity, but it has minor effects on the carrier densities of electrons and holes as well as the shapes of the Fermi surfaces. Correspondingly, the structural transition and magnetic fluctuations in $Fe_{1-x}Cu_xSe$ change slowly with x.

DOI: 10.1103/PhysRevB.103.174510

I. INTRODUCTION

Among iron-based superconductors (SCs), even the similar electric structures between FeAs-based SCs and FeSe with hole pockets near the Γ point and electron pockets near the *M* point of Brillouin zone [1–4], the latter, with the simplest structure (only two FeSe layers in one unit cell without a carrier reservoir), still attracts a great deal of attention due to its unique physical properties. For example, FeSe exhibits a structural transition (nematic ordering transition) at $T_s \sim 90$ K but without the appearance of magnetic order [2,5]. Without doping, FeSe shows a superconducting transition below the critical temperature $T_c \sim 8$ K at ambient pressure [6]. Furthermore, pressure, intercalation (heavily electron doping), and reduced dimensionality (monolayer FeSe film on $SrTiO_3$) can enhance T_c remarkably [7–14]. More importantly, the heavily electron doped FeSe-based SCs raise a great challenge to the proposed spin-fluctuation-mediated pairing mechanism in FeAs-based and FeSe SCs (denoted by $s_\pm$ pairing) [15] because the hole pockets crucial to this pairing mechanism are absent in these compounds [16].

Substitution is an effective way to tune superconductivity and explore the superconducting mechanism in iron-based SCs [17,18]. Although isovalent Te doping at the Se site can enhance T_c significantly with the suppression of T_s [19,20], similar to that in $BaFe_2(As_{1-x}P_x)$ [21], the substitution effects of transition metals at the Fe site in FeSe have many exotic features when compared to those in FeAs-based SCs. Taking Co and Ni doping as examples, these dopants can induce superconductivity in FeAs-based SCs [18]; however, they suppress T_c of FeSe rapidly [20,22]. Cu doping is even more exotic. It not only destroys the bulk superconductivity of the $Fe_{1-x}Cu_xSe$ polycrystal completely at an extremely low concentration ($x \sim 1.5\%$) but also induces a metal-insulator transition (MIT; $x \sim 4\%$) [23,24], which is different from Co- and Ni-doped FeSe and Cu-doped FeAs-based SCs [18,20,22,25]. Theoretical calculations suggest that the Cu ions in $Fe_{1-x}Cu_xSe$ have a nominal d^{10} configuration rather than a d^9 one; thus, they are a source of strong disorder scattering, leading to the suppression of T_c and the emergence of MIT [26].

Because of the absence of high-quality single crystals, however, details about the effects of Cu doping on the physical properties of normal and superconducting states, especially on T_s, are still lacking. In this work, we carry out a systematic study of the physical properties of a series of Cu-doped FeSe single crystals. We find that the superconducting transition is suppressed more quickly than the structural transition with Cu doping. Furthermore, the MIT appears at the higher doping level. Transport measurements further show that the hole-type carriers become dominant with Cu doping and the dramatic suppression of T_c, which may originate from strong disorder scattering instead of the change in carrier density with the introduction of Cu.

II. EXPERIMENT

Single crystals of $Fe_{1-x}Cu_xSe$ were grown by a horizontal flux technique using elemental Fe, Cu, Se, and a eutectic mixture of chlorine salts, similar to the growth procedure for undoped FeSe single crystals [12,27]. The elemental analysis was performed using an energy-dispersive x-ray spectroscopy (EDX) analysis. Electrical transport measurements were carried out in a Quantum Design physical property measurement system (PPMS-14T). The *ab*-plane resistivity $\rho_{xx}(\mu_0 H)$ and

*hlei@ruc.edu.cn

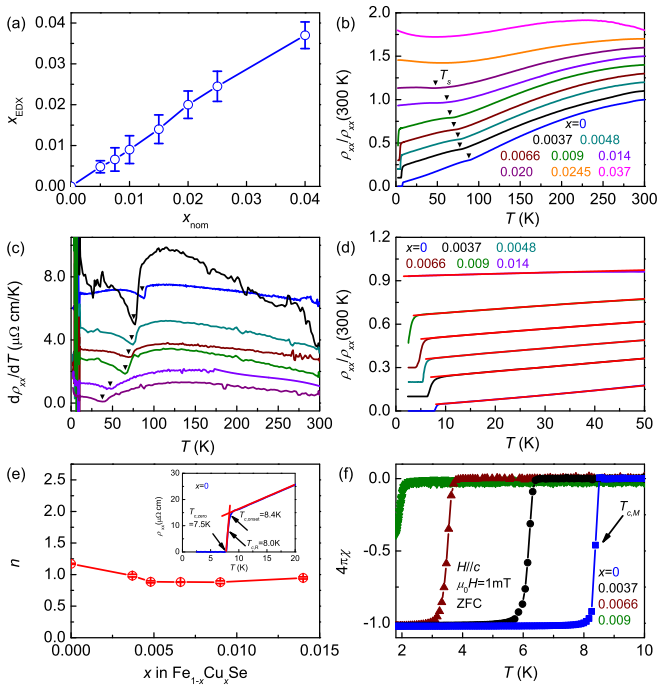

FIG. 1. (a) Relationship between the nominal concentration of Cu $x_{\rm nom}$ and the actual one $x_{\rm EDX}$ determined by EDX in $Fe_{1-x}Cu_xSe$ single crystals. (b) Temperature dependence of normalized in-plane resistivity $\rho_{xx}(T)/\rho_{xx}(300\ {\rm K})$. Each curve is shifted by 0.1 for clarity. The solid triangles indicate the T_s which is defined as the peak position of the first derivative of ρ. (c) $d\rho_{xx}/dT$ as a function of T. (d) Enlarged part of normalized resistivity curves in the low-temperature region with fittings (red lines) using the formula $B + AT^n$. (e) The fitted n values as a function of $x_{\rm EDX}$. Inset: the $\rho_{xx}(T)$ curve near the superconducting transition region for FeSe ($x = 0$). (f) Temperature dependence of dc magnetic susceptibility $4\pi\chi$ at $\mu_0H = 1$ mT for $H\|c$ with the ZFC mode.

Hall electrical resistivity $\rho_{yx}(\mu_0H)$ were measured using a standard four-probe method on rectangular-shaped single crystals with current flowing in the *ab* plane, while the magnetic field was applied along the *c* axis. $\rho_{yx}(\mu_0H)$ was obtained from the difference in the off-diagonal resistivity measured at the positive and negative fields in order to remove the contribution of $\rho_{xx}(\mu_0H)$ due to the voltage probe misalignment, i.e., $\rho_{yx}(\mu_0H) = [\rho_{yx}(T, +\mu_0H) - \rho_{yx}(T, -\mu_0H)]/2$. Magnetization measurements were performed in a Quantum Design magnetic property measurement system (MPMS3).

III. RESULTS AND DISCUSSION

Figure 1(a) shows the actual Cu concentration $x_{\rm EDX}$ determined by the EDX measurement as a function of the nominal doping level $x_{\rm nom}$. The values of $x_{\rm EDX}$ are taken as the average at several positions on each crystal. Even for such a low doping level at which the EDX results may be less accurate, there is an unambiguous linear dependence of $x_{\rm EDX}$ on $x_{\rm nom}$. It strongly indicates the amount of Cu doped into FeSe is close to the expected one. In addition, the EDX mapping analysis of $Fe_{1-x}Cu_xSe$ crystals confirms that the distribution of doped Cu is homogeneous [28]. Thus, we will use $x_{\rm EDX}$ (noted as x) for the following discussion. The temperature dependence of normalized *ab*-plane resistivity $\rho_{xx}(T)/\rho_{xx}(300\ {\rm K})$ for $Fe_{1-x}Cu_xSe$ single crystals is shown in Fig. 1(b). For the undoped FeSe, the resistivity anomaly related to the structural transition appears at $T_s \sim 89$ K [determined by the dip in $d\rho_{xx}/dT$; Fig. 1(c)], consistent with previous results [2,5]. With increasing the content of Cu, T_s shifts to a lower temperature slowly and cannot be observed above 2 K at $x \sim 0.0245$. Figure 1(d) shows the enlarged part of the normalized resistivity curves in the low-temperature region ($T < 50$ K). It can be seen that the normal-state resistivity can be fitted well by using the formula $\rho_{xx}(T)/\rho_{xx}(300\ {\rm K}) = \rho_0 + AT^n$ (red lines). As shown in Fig. 1(e), the fitted values of n are insensitive to x and close to 1, significantly deviating from the Fermi liquid behavior. Such quasi-T-linear resistivity is very similar to that in $FeSe_{1-x}S_x$ at relatively high temperatures and can be linked to the spin fluctuations [29,30]. It suggests that Cu doping could have a minor influence on the magnetic fluctuations in FeSe, consistent with the NMR results [31]. In contrast, the obtained ρ_0 increases with x in general [28], and it indicates that the doped Cu introduces disorder or defects, playing a role in the scattering centers of the carriers. With further decreasing the temperature, there is a sharp drop in the resistivity curve, corresponding to the superconducting transition. For FeSe, the onset temperature of the superconducting transition $T_{c,\rm onset}$ is determined by the intersecting point of the linear extrapolations of $\rho_{xx}(T)$ curves in normal and superconducting states, $T_{c,\rm zero}$ is where the resistivity becomes zero, and $T_{c,\rm R}$ is the temperature at which the $\rho_{xx}(T) = 50\%\rho_{xx}(T_{c,\rm onset})$. The corresponding temperatures are 8.4, 8.0, and 7.5 K, respectively [inset in Fig. 1(e)]. By increasing the content of Cu, both $T_{c,\rm onset}$ and $T_{c,\rm zero}$ are suppressed to lower temperatures. $T_{c,\rm zero}$ and $T_{c,\rm onset}$ cannot be observed above 2 K when $x \geqslant 0.009$ and $x \geqslant 0.014$, respectively. It has to be noted that although suppression of both superconductivity and structural transitions in FeSe occurs by partial replacement of Fe with Cu, the influence of Cu doping is distinctly different: T_c is suppressed more quickly than T_s. On the other hand, at $x = 0.037$, the negative slopes of resistivity emerge at low and high temperatures; that is, insulating behavior appears. The monotonic decrease of the residual resistivity ratio [RRR = $\rho_{xx}(300\ {\rm K})/\rho_{xx}(9\ {\rm K})$] also reflects the evolution from the metallic state to the insulator one with Cu doping [28]. It probably originates from the Anderson localization of charge carriers due to the disorder induced by Cu doping [26].

Figure 1(f) shows the zero-field-cooling (ZFC) dc magnetic susceptibility $4\pi\chi(T)$ of $Fe_{1-x}Cu_xSe$ single crystals at $\mu_0H = 1$ mT for $H\|c$. $T_{c,M}$ is determined from the 50% point of the diamagnetic signal in the $4\pi\chi(T)$ curve. It is obvious that $T_{c,M}$ is suppressed quickly when introducing a small amount of Cu into the Fe site, consistent with the resistivity measurement as well as the previous results for the $Fe_{1-x}Cu_xSe$ polycrystal [23,24]. Strong suppression of T_c is also observed in Co- and Ni-doped FeSe, but this trend is distinct different from the mild suppression (even slight enhancement) of T_c in $FeSe_{1-x}S_x$ [20,22,30,32,33]. It implies that the aliovalent doping into the Fe plane has a more significant influence on physical properties than the isovalent substitution in the Se site. Moreover, after taking into account the demagnetization effect of the crystals, the

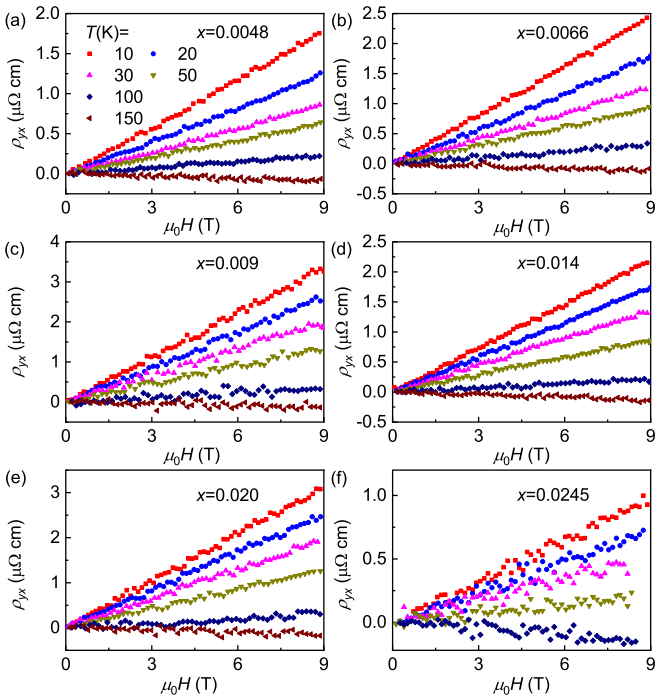

FIG. 2. (a)–(f) Field dependence of Hall resistivity $\rho_{yx}(\mu_0 H)$ up to $\mu_0 H = 9$ T at various temperatures for $Fe_{1-x}Cu_xSe$ with $x = 0.0048$, 0.0066, 0.009, 0.014, 0.020, and 0.0245, respectively.

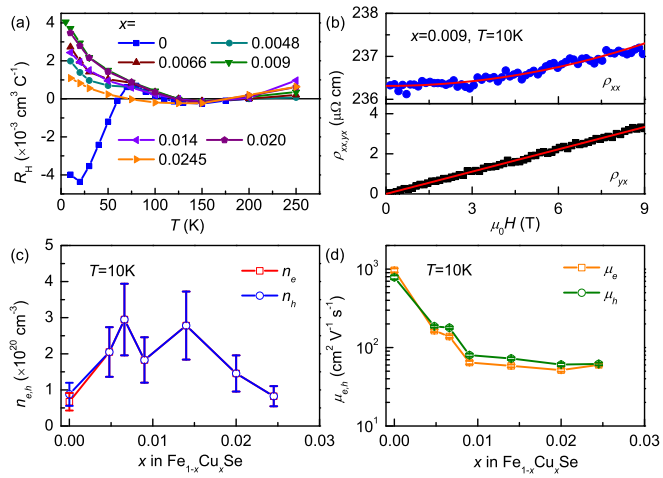

FIG. 3. (a) Temperature dependence of the Hall coefficient $R_H(T)$ for $Fe_{1-x}Cu_xSe$. The values of $R_H(T)$ are obtained from the linear fits of $\rho_{yx}(\mu_0 H)$ curves. (b) The fits of magnetoresistance and Hall resistivity of $Fe_{1-x}Cu_xSe$ with $x = 0.009$ at 10 K using a compensated two-band model. (c) $n_{e,h}(T)$ and (d) $\mu_{e,h}(T)$ as a function of x at 10 K.

superconducting volume fractions estimated from the ZFC $4\pi\chi(T)$ curves are still about 100%, except for the sample with $x = 0.009$, limited by the lowest measured temperature. These results indicate that the bulk superconductivity persists in $Fe_{1-x}Cu_xSe$ single crystals even with the decrease of T_c. Thus, the suppression of T_c with Cu doping should be a bulk effect.

The field dependence of Hall resistivity $\rho_{yx}(\mu_0 H)$ at various temperatures is investigated to get more information about the carriers in $Fe_{1-x}Cu_xSe$ single crystals. As shown in Fig. 2, all of the $\rho_{yx}(\mu_0 H)$ curves for $Fe_{1-x}Cu_xSe$ single crystals show a similar linear dependence on magnetic field up to 9 T in the whole temperature range, obviously different from the bent curves of FeSe at low temperature [34]. At low temperature, the values of $\rho_{yx}(\mu_0 H)$ are positive for all samples. With increasing temperatures, the slopes of the $\rho_{yx}(\mu_0 H)$ curves become smaller, and the values of $\rho_{yx}(\mu_0 H)$ change from positive to negative. The behavior of $\rho_{yx}(\mu_0 H)$ for $Fe_{1-x}Cu_xSe$ is different from that of $Fe_{1-x}Co_xSe$, in which all of the $\rho_{yx}(\mu_0 H)$ curves exhibit negative slopes between 10 and 180 K when the doping level of Co is in the range of 0.010–0.075 [35].

Figure 3(a) summarizes the temperature dependence of the Hall coefficient $R_H(T) \equiv \rho_{yx}(\mu_0 H)/\mu_0 H$ determined from the linear fits of the $\rho_{yx}(T, \mu_0 H)$ curves of $Fe_{1-x}Cu_xSe$ with various Cu contents. At high temperatures, the amplitude of positive R_H is almost unchanged with varying the doping level of Cu. In contrast, at low temperatures its value depends on x weakly. At first glance, positive R_H with linear field dependence of $\rho_{yx}(\mu_0 H)$ implies that the substitution of Cu for Fe leads to the hole doping. But the fits using the single-band model give unreasonably high hole concentrations ($\sim$1.7–5.7 $\times 10^{21}$ cm^{-3}), one order of magnitude higher than those in FeSe [34]. Moreover, previous theoretical calculations suggest that even though the valence state of Cu is +1, Cu substitution leads to electron doping [26]. Because FeSe is a nearly compensated semimetal, i.e., the electron and hole concentrations $n_{e,h}$ are almost identical, and x is very low, which may only slightly change $n_{e,h}$ [26], we can analyze the magnetoresistance and Hall resistivity of $Fe_{1-x}Cu_xSe$ in the framework of the two-band model with a compensation condition ($n_e = n_h$) [36],

$$\rho_{xx} = \frac{1}{n_e(\mu_e + \mu_h)e}[1 + \mu_h\mu_e B^2] = \rho_{xx,0}[1 + \mu_h\mu_e B^2], \tag{1}$$

$$\rho_{yx} = \frac{\mu_0 H}{n_e e}\frac{\mu_h - \mu_e}{\mu_h + \mu_e}, \tag{2}$$

where μ_e and μ_h are the mobilities of electrons and holes, respectively. $\rho_{xx,0}$ is the zero-field *ab*-plane resistivity. All $\rho_{xx}(\mu_0 H)$ and $\rho_{yx}(\mu_0 H)$ curves can be fitted quite well using Eqs. (1) and (2) with the two-band model. Figure 3(b) shows an example of simultaneous fits of $\rho_{xx}(\mu_0 H)$ and $\rho_{yx}(\mu_0 H)$ for the sample with $x = 0.009$ at 10 K. The fits of $\rho_{xx}(\mu_0 H)$ for other samples are shown in the Supplemental Material [28]. The obtained $n_{e,h}(T)$ and $\mu_{e,h}(T)$ as a function of x are shown in Figs. 3(c) and 3(d). It has to be mentioned that the fitted values of $n_{e,h}(T)$ and $\mu_{e,h}(T)$ for FeSe are obtained using the two-band model when setting $n_e(T)$ and $n_h(T)$ as two independent parameters. The variation of $n_{e,h}(T)$ with x might partially originate from the measurement uncertainties of the geometric size of the samples, especially for the thickness of the thin crystals. In contrast, both $\mu_e(T)$ and $\mu_h(T)$ decrease dramatically with the increase of x. This is consistent with the results of theoretical calculations in which doped Cu ions can be regarded as a source of strong scattering, which could lead to the Anderson localization and thus the

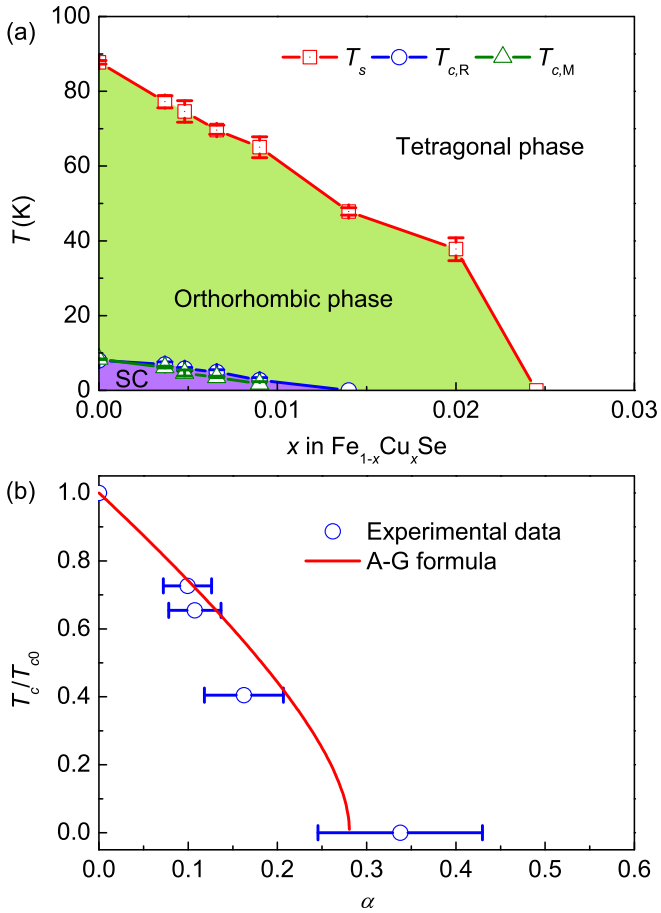

FIG. 4. (a) A composition vs temperature phase diagram of $Fe_{1-x}Cu_xSe$ single crystals. The red squares, blue circles, and green triangles represent T_s, $T_{c,\mathrm{R}}$, and $T_{c,\mathrm{M}}$ determined from resistivity and magnetization measurements. The error bars of $T_{c,\mathrm{R}}$ and $T_{c,\mathrm{M}}$ represent the superconducting transition widths ($\Delta T_{c,\mathrm{R}} = T_{c,\mathrm{onset}} - T_{c,\mathrm{zero}}$ and $\Delta T_{c,\mathrm{M}} = 10\%$–$90\%$ values of $4\pi\chi$ at 1.8 K). The error bars of T_s are estimated from the widths of the structural transitions in the $\rho_{xx}(T)$ curves. SC: superconducting state. (b) T_c/T_{c0} vs α calculated using Eq. (3). Here T_{c0} and T_c represent $T_{c,\mathrm{onset}}$ of FeSe- and Cu-doped FeSe, respectively. The error bars originate from the different m^* of hole and electron pockets. The red line represents the result calculated using the AG formula.

appearance of the insulating phase even at a very low doping level [26]. This is obviously different from the effect of Co or Ni substitution, in which the normal-state resistivity still shows a metallic behavior [20,35] because these dopants can still keep coherent electronic structures [26]. Moreover, when compared to FeSe in which the dominant carriers are electrons with higher mobility [34], μ_h becomes larger than μ_e even with a tiny amount of Cu doping, resulting in the positive slopes of the $\rho_{yx}(\mu_0 H)$ curves in the low-temperature region. This result suggests that the scattering effect of Cu ions on electrons may be stronger than that on holes.

The phase diagram of $Fe_{1-x}Cu_xSe$ single crystals is plotted in Fig. 4. $T_{c,\mathrm{R}}$ and $T_{c,\mathrm{M}}$ determined from resistivity and magnetization measurements are consistent with each other, and the purple area represents the region of the superconducting state. Below T_s, $Fe_{1-x}Cu_xSe$ has an orthorhombic phase, and above it, the tetragonal phase exists. The most striking feature is that when superconductivity is suppressed quickly with Cu doping and disappears below 2 K at the critical concentration $x \sim 0.014$, T_s is still very high (about 48 K), which is suppressed completely until $x = 0.0245$. In contrast, both superconducting and structural transitions disappear simultaneously at a higher doping level ($x = 0.036$) in Co-doped FeSe [35]. The Co doping introduces extra electrons that could the weaken Fermi surface (FS) nesting and suppress both transitions [35]. Different from $Fe_{1-x}Co_xSe$, the above analysis suggests that the small amount of Cu doping may not significantly change the carrier density, i.e., E_F; thus, it has a minor effect on the shapes of FSs, which are important to the structural transition (nematic ordering) [37]. But Cu doping induces strong disorder scattering indeed, especially for electron-type carriers [26], which could be detrimental to superconductivity. This is also consistent with the faster suppression of T_c than those in $Fe_{1-x}Co_xSe$ and $Fe_{1-x}Ni_xSe$ at the same doping level [20,35].

Next, we discuss the pair-breaking mechanism of $Fe_{1-x}Cu_xSe$. According to the $s_\pm$ scenario, the nonmagnetic impurity scattering between bands with different signs of the order parameter suppresses T_c in the same way as a magnetic impurity in a single-band BCS superconductor [38–40]. Thus, the suppression of T_c by nonmagnetic impurities should obey the Abrikosov-Gor'kov (AG) formula [41]

$$-\ln(T/T_{c0}) = \psi\left(\frac{1}{2} + \frac{\alpha T_{c0}}{2T}\right) - \psi\left(\frac{1}{2}\right), \tag{3}$$

where T_{c0} and T_c are $T_{c,\mathrm{onset}}$ of the undoped and doped FeSe samples, respectively, $\psi(x)$ is the digamma function, and α is the pair-breaking parameter. The red line in Fig. 4(b) shows the relationship between $T_c/T_{c,0}$ and α calculated using the AG formula, which indicates that T_c vanishes at $\alpha_{c,\mathrm{theory}} = 0.28$. According to the theoretical calculations based on the five-orbital model [42,43], α can be expressed as

$$\alpha = \frac{z\hbar\Gamma}{2\pi k_\mathrm{B} T_{c0}}, \tag{4}$$

where $z = m/m^*$ is the renormalization factor with band mass m and effective masses m^* and Γ is the electron scattering rate. The angle-resolved photoemission spectroscopy (ARPES) measurements indicate that m^*/m is between 3 and 9 [44]; when taking $m^*/m = 6$, $z = 0.17$. Γ can be calculated using the relation $\Gamma = n_e e^2 \Delta\rho_0/m^*$, where $\Delta\rho_0$ is the difference in ρ_0 between the Cu-doped and Cu-free FeSe crystals [43]. According to the quantum oscillation results, m^* are about $4m_e$ and $7m_e$–$8m_e$ for hole and electron pockets [34], respectively, where m_e is the electron mass, in agreement with the ARPES results [45]. Thus, we take $5.5m_e$ as the averaged value of m^* from both bands. As shown in Fig. 4(b), α_c for $Fe_{1-x}Cu_xSe$ is much smaller than those in FeAs-based SCs [17], and the relationship between T_c/T_{c0} and α calculated using Eq. (4) is in line with the results obtained from the AG formula. It indicates that the impurity effect of Cu in FeSe can be well explained by the $s_\pm$ scenario, consistent with the measurement results of scanning tunneling microscopy [46].

IV. CONCLUSION

In summary, a series of $Fe_{1-x}Cu_xSe$ single crystals were grown successfully using the molten-salt flux method. The resistivity and magnetization measurements indicated that bulk T_c is suppressed much faster than T_s with Cu doping and a MIT emerges at higher Cu content ($x \geqslant 0.037$). On the other hand, the exponent of the temperature dependence of $\rho_{xx}(T)$ is close to 1 when $x < 0.015$. Based on the analysis of the field dependence of Hall and *ab*-plane resistivities using the two-band model with the compensation condition, we found that $n_{e,h}(T)$ do not change significantly with x, while $\mu_{n,h}(T)$ decrease dramatically with $\mu_h > \mu_n$ at 10 K. All of these results suggest that at small x, the strong disorder scattering of Cu ions, especially for electron-type carriers, remarkably suppresses T_c, while T_s and magnetic fluctuation are not susceptible to the Cu doping because of the little change in carrier concentrations. Further analysis suggested that the pair-breaking rate of nonmagnetic Cu defects is consistent with the prediction of the $s_\pm$ model, providing strong evidence of the gap structure of $s_\pm$ in FeSe.

ACKNOWLEDGMENTS

This work was supported by the Beijing Natural Science Foundation (Grant No. Z200005), the Ministry of Science and Technology of China (Grants No. 2018YFE0202600 and No. 2016YFA0300504), the National Natural Science Foundation of China (Grants No. 11774423 and No. 11822412), and the Fundamental Research Funds for the Central Universities and Research Funds of Renmin University of China (Grants No. 18XNLG14 and No. 19XNLG17).

[1] A. Subedi, L. Zhang, D. J. Singh, and M. H. Du, Phys. Rev. B **78**, 134514 (2008).
[2] K. Nakayama, Y. Miyata, G. N. Phan, T. Sato, Y. Tanabe, T. Urata, K. Tanigaki, and T. Takahashi, Phys. Rev. Lett. **113**, 237001 (2014).
[3] A. I. Coldea and M. D. Watson, Annu. Rev. Condens. Matter Phys. **9**, 125 (2018).
[4] G. R. Stewart, Rev. Mod. Phys. **83**, 1589 (2011).
[5] T. M. McQueen, A. J. Williams, P. W. Stephens, J. Tao, Y. Zhu, V. Ksenofontov, F. Casper, C. Felser, and R. J. Cava, Phys. Rev. Lett. **103**, 057002 (2009).
[6] F. C. Hsu, J. Y. Luo, K. W. Yeh, T. K. Chen, T. W. Huang, P. M. Wu, Y. C. Lee, Y. L. Huang, Y. Y. Chu, D. C. Yan, and M. K. Wu, Proc. Natl. Acad. Sci. USA **105**, 14262 (2008).
[7] S. Medvedev, T. M. McQueen, I. A. Troyan, T. Palasyuk, M. I. Eremets, R. J. Cava, S. Naghavi, F. Casper, V. Ksenofontov, G. Wortmann, and C. Felser, Nat. Mater. **8**, 630 (2008).
[8] Y. Mizuguchi, F. Tomioka, S. Tsuda, T. Yamaguchi, and Y. Takano, Appl. Phys. Lett. **93**, 152505 (2008).
[9] J. G. Guo, S. F. Jin, G. Wang, S. C. Wang, K. X. Zhu, T. T. Zhou, M. He, and X. L. Chen, Phys. Rev. B **82**, 180520(R) (2010).
[10] T. P. Ying, X. L. Chen, G. Wang, S. F. Jin, T. T. Zhou, X. F. Lai, H. Zhang, and W. Y. Wang, Sci. Rep. **2**, 426 (2012).
[11] M. Burrard-Lucas, D. G. Free, S. J. Sedlmaier, J. D. Wright, S. J. Cassidy, Y. Hara, A. J. Corkett, T. Lancaster, P. J. Baker, S. J. Blundell, and S. J. Clarke, Nat. Mater. **12**, 15 (2013).
[12] S. S. Sun, S. H. Wang, R. Yu, and H. C. Lei, Phys. Rev. B **96**, 064512 (2017).
[13] X. F. Lu, N. Z. Wang, H. Wu, Y. P. Wu, D. Zhao, X. Z. Zeng, X. G. Luo, T. Wu, W. Bao, G. H. Zhang, F. Q. Huang, Q. Z. Huang, and X. H. Chen, Nat. Mater. **14**, 325 (2015).
[14] Q. Y. Wang, Z. Li, W. H. Zhang, Z. C. Zhang, J. S. Zhang, W. Li, H. Ding, Y. B. Ou, P. Deng, K. Chang, J. Wen, C. L. Song, K. He, J. F. Jia, S. H. Ji, Y. Y. Wang, L. L. Wang, X. Chen, X. C. Ma, and Q. K. Xue, Chin. Phys. Lett. **29**, 037402 (2012).
[15] I. I. Mazin, D. J. Singh, M. D. Johannes, and M. H. Du, Phys. Rev. Lett. **101**, 057003 (2008).
[16] L. Zhao *et al.*, Nat. Commun. **7**, 10608 (2016).
[17] J. Li, Y. F. Guo, Z. R. Yang, K. Yamaura, E. Takayama-Muromachi, H. B. Wang, and P. H. Wu, Supercond. Sci. Technol. **29**, 053001 (2016).
[18] P. C. Canfield and S. L. Bud'ko, Annu. Rev. Condens. Matter Phys. **1**, 27 (2010).
[19] K. W. Yeh, T. W. Huang, Y. L. Huang, T. K. Chen, F. C. Hsu, P. M. Wu, Y. C. Lee, Y. Y. Chu, C. L. Chen, J. Y. Luo, D. C. Yan, and M. K. Wu, Europhys. Lett. **84**, 37002 (2008).
[20] Y. Mizuguchi, F. Tomioka, S. Tsuda, T. Yamaguchi, and Y. Takano, J. Phys. Soc. Jpn. **78**, 074712 (2009).
[21] S. Kasahara, T. Shibauchi, K. Hashimoto, K. Ikada, S. Tonegawa, R. Okazaki, H. Shishido, H. Ikeda, H. Takeya, K. Hirata, T. Terashima, and Y. Matsuda, Phys. Rev. B **81**, 184519 (2010).
[22] S. B. Zhang, H. C. Lei, X. D. Zhu, G. Li, B. S. Wang, L. J. Li, X. B. Zhu, W. H. Song, Z. R. Yang, and Y. P. Sun, Physica C (Amsterdam, Neth.) **469**, 1958 (2009).
[23] A. J. Williams, T. M. McQueen, V. Ksenofontov, C. Felser, and R. J. Cava, J. Phys.: Condens. Matter **21**, 305701 (2009).
[24] T. W. Huang, T. K. Chen, K. W. Yeh, C. T. Ke, C. L. Chen, Y. L. Huang, F. C. Hsu, M. K. Wu, P. M. Wu, M. Avdeev, and A. J. Studer, Phys. Rev. B **82**, 104502 (2010).
[25] L. Y. Xing, H. Miao, X. C. Wang, J. Ma, Q. Q. Liu, Z. Deng, H. Ding, and C. Q. Jin, J. Phys.: Condens. Matter **26**, 435703 (2014).
[26] S. Chadov, D. Schärf, G. H. Fecher, C. Felser, L. Zhang, and D. J. Singh, Phys. Rev. B **81**, 104523 (2010).
[27] P. S. Wang, S. S. Sun, Y. Cui, W. H. Song, T. R. Li, R. Yu, H. C. Lei, and W. Q. Yu, Phys. Rev. Lett. **117**, 237001 (2016).
[28] See Supplemental Material at http://link.aps.org/supplemental/10.1103/PhysRevB.103.174510 for the EDX mapping of $Fe_{1-x}Cu_xSe$ crystals, the x dependence of ρ_0 and RRR, and the field dependence and two-band model fits of $\rho_{xx}(\mu_0 H)$ at 10 K for different x.
[29] M. Bristow, P. Reiss, A. A. Haghighirad, Z. Zajicek, S. J. Singh, T. Wolf, D. Graf, W. Knafo, A. McCollam, and A. I. Coldea, Phys. Rev. Research **2**, 013309 (2020).
[30] S. Licciardello, J. Buhot, J. Lu, J. Ayres, S. Kasahara, Y. Matsuda, T. Shibauchi, and N. E. Hussey, Nature (London) **567**, 213 (2019).

[31] B. L. Young, J. Wu, T. W. Huang, K. W. Yeh, and M. K. Wu, Phys. Rev. B **81**, 144513 (2010).
[32] M. Abdel-Hafiez, Y. J. Pu, J. Brisbois, R. Peng, D. L. Feng, D. A. Chareev, A. V. Silhanek, C. Krellner, A. N. Vasiliev, and X. J. Chen, Phys. Rev. B **93**, 224508 (2016).
[33] M. D. Watson, T. K. Kim, A. A. Haghighirad, S. F. Blake, N. R. Davies, M. Hoesch, T. Wolf, and A. I. Coldea, Phys. Rev. B **92**, 121108(R) (2015).
[34] M. D. Watson, T. Yamashita, S. Kasahara, W. Knafo, M. Nardone, J. Béard, F. Hardy, A. McCollam, A. Narayanan, S. F. Blake, T. Wolf, A. A. Haghighirad, C. Meingast, A. J. Schofield, H. V. Löhneysen, Y. Matsuda, A. I. Coldea, and T. Shibauchi, Phys. Rev. Lett. **115**, 027006 (2015).
[35] T. Urata, Y. Tanabe, K. K. Huynh, Y. Yamakawa, H. Kontani, and K. Tanigaki, Phys. Rev. B **93**, 014507 (2016).
[36] J. M. Ziman, *Electrons and Phonons*, Classics Series (Oxford University Press, New York, 2001).
[37] A. V. Chubukov, R. M. Fernandes, and J. Schmalian, Phys. Rev. B **91**, 201105(R) (2015).
[38] A. V. Chubukov, D. V. Efremov, and I. Eremin, Phys. Rev. B **78**, 134512 (2008).
[39] A. A. Golubov and I. I. Mazin, Phys. Rev. B **55**, 15146 (1997).
[40] A. A. Golubov and I. I. Mazin, Physica C (Amsterdam, Neth.) **243**, 153 (1995).
[41] A. A. Abrikosov and L. P. Gor'kov, Sov. Phys. JETP **12**, 1243 (1961).
[42] S. Onari and H. Kontani, Phys. Rev. Lett. **103**, 177001 (2009).
[43] Q. Deng, X. Ding, S. Li, J. Tao, H. Yang, and H.-H. Wen, New J. Phys. **16**, 063020 (2014).
[44] J. Maletz, V. B. Zabolotnyy, D. V. Evtushinsky, S. Thirupathaiah, A. U. B. Wolter, L. Harnagea, A. N. Yaresko, A. N. Vasiliev, D. A. Chareev, A. E. Böhmer, F. Hardy, T. Wolf, C. Meingast, E. D. L. Rienks, B. Büchner, and S. V. Borisenko, Phys. Rev. B **89**, 220506(R) (2014).
[45] D. Liu *et al.*, Phys. Rev. X **8**, 031033 (2018).
[46] P. O. Sprau, A. Kostin, A. Kreisel, A. E. Böhmer, V. Taufour, P. C. Canfield, S. Mukherjee, P. J. Hirschfeld, B. M. Andersen, and J. C. S. Davis, Science **357**, 75 (2017).